Wind and Structures, *Vol. 29, No. 6 (2019) 431-440*
DOI: https://doi.org/10.12989/was.2019.29.6.431

Influence of structure coupling effect on damping coefficient of offshore wind turbine blades

Jianping Zhang*[1], Zhen Gong[2], Haolin Li[1], Mingqiang Wang[2], Zhiwei Zhang[3] and Fengfeng Shi[2]

[1]School of Mechanical Engineering, University of Shanghai for Science and Technology, Shanghai 200093, China
[2]College of Energy and Mechanical Engineering, Shanghai University of Electric Power, Shanghai 200090, China
[3]Shanghai Green Environmental Protection Energy Co., Ltd, Shanghai 200433, China

(Received November 22, 2018, Revised May 9, 2019, Accepted May 27, 2019)

Abstract. The aim of this study was to explore the influence of structure coupling effect on structural damping of blade based on the blade vibration characteristic. For this purpose, the scaled blade model of NREL 5 MW offshore wind turbine was processed and employed in the wind tunnel test to validate the reliability of theoretical and numerical models. The attenuation curves of maximum displacement and the varying curves of equivalent damping coefficient of the blade under the rated condition were respectively compared and analyzed by constructing single blade model and whole machine model. The attenuation law of blade dynamic response was obtained and the structure coupling effect was proved to exert a significant influence on the equivalent damping coefficient. The results indicate that the attenuation trend of the maximum displacement response curve of the single blade varies more obviously with the increase of elastic modulus as compared to that under the structure coupling effect. In contrast to the single blade model, the varying curve of equivalent damping coefficient with the period is relatively steep for the whole machine model. The findings are of great significance to guide the structure design and material selection for wind turbine blades.

Keywords: offshore wind turbines; damping coefficient; structure coupling effect; wind tunnel test; elastic modulus

1. Introduction

At present, owing to the vital role of damping on structural vibration, the research on damping has a high value in engineering applications, and the related technologies have been widely applied in aerospace, machinery, energy and other industries (Magalhaes *et al*. 2010, Eichler *et al*. 2011, Quan *et al*. 2016, Zhang *et al*. 2016, Lu *et al*. 2018). With the large-scale development of offshore wind turbines, the blades become longer and longer. In the operation process of wind turbine, the long blade is prone to the nonlinear vibration due to the fluid-structure interaction (FSI). In the vibration control of structural systems, structural damping plays an important role in preventing the blade aeroelastic instability (Ren and Liu 2013, Chen *et al*. 2017) including stall flutter and coupled flap-lag flutter, etc., and thereby more and more engineers and technicians attach importance to structural damping. Therefore, the research on the blade damping is of great significance for the design of large-scale blades and the safe and stable operation of wind turbines.

In the previous study of wind turbines, the influence of the whole structure vibration on the damping analysis of the individual component is generally ignored. Zhang and He (2015) developed a three dimensional structural dynamic model of the tower of wind turbine, and explored the influence of structural damping on the tower vibration. Liu *et al*. (2013) analyzed the aerodynamic damping and structural damping, and investigated the dynamic response of tubular tower of wind turbine subjected to the time-varying load. Meng and Sun (2017) put forward a new damping structure with the blade, and the comparison diagrams of swing and wave velocity responses and their displacement responses between conditions with and without the new damping structure were gained, which indicates that the property of vibration suppression of wind turbine blades with the new damping structure is significantly improved. Basu *et al*. (2016) proposed a new type of passive vibration control damper for controlling edgewise vibrations of wind turbine blades, and evaluated the performance of the damper by applying a reduced 2-DOF non-linear model which was used for tuning the circular liquid column damper attached to a rotating wind turbine blade, ignoring the coupling between the blade and the tower. However, the influence of structural coupling effect on the damping of the single component is not discussed in some literature (Tran and Kim 2015, Pascu *et al*. 2017, Zendehbad *et al*. 2017) based on the whole structural damping analysis.

In order to accurately reflect the dynamic characteristics of wind turbine blades under actual working condition, the influence of structure coupling effect on the damping coefficient of the single component should not be ignored. In view of this, aiming at large-scale offshore wind turbines, equivalent damping analysis of the blade with different elasticity modulus under FSI was carried out based on the single blade model and whole machine model, and the numerical results reveal the attenuation law of the blade dynamic response, which can provide theoretical basis and

∗Corresponding author, Professor
E-mail: jpzhanglzu@163.com

http://www.techno-press.com/journals/was&subpage=7 ISSN: 1226-6116 (Print), 1598-6225 (Online)

technical guidance for the safety operation and reliability design of wind turbines.

2. Basic theories

2.1 Governing equations of fluid domain

The continuity equation and momentum equation built by ALE method can be respectively expressed as (Zhang and Dong 1998)

$$\frac{\partial \rho}{\partial t}+\frac{\partial \rho u_i}{\partial x_i}=0 \tag{1}$$

$$\frac{\partial(\rho u_j)}{\partial t}+\frac{\partial(\rho u_j)}{\partial x_i}(u_i-u_{gi})=\frac{\partial}{\partial x_i}\left[(\mu+\mu_t)\frac{\partial u_j}{\partial x_i}\right]-\frac{\partial P}{\partial x_j}+S_j \tag{2}$$

where ρ and P are respectively the density and pressure of fluid. u_i and u_j stand for speed components of fluid in each direction, and the indexes of i, j range from 1 to 3. u_{gi} is the movement speed of grid in fluid domain and S_j is the generalized source term.

2.2 Motion equations of structure domain

The discrete motion differential equation with geometric nonlinearity taken into account is defined as

$$[M][\ddot{x}]_t+[C][\dot{x}]_t+[\bar{P}]_t=[F(t)] \tag{3}$$

where $[\dot{x}]_t$ and $[\ddot{x}]_t$ are respectively the velocity and accelerated velocity at the time t, $[\dot{x}]=[\dot{u}, \dot{v}, \dot{w}]^T$. $[M]$ and $[C]$ represent the mass matrix and the damping matrix respectively. $[F(t)]$ is the column vector of load on structure, and $[\bar{P}]_t$ is the nonlinear term that consists of both the displacement $[x]_t$ and stiffness $[K]_t$.

In finite element analysis, the balance equation corresponding to Eq. (3) at the time $t+\Delta t$ can be described as

$$[F(t)]_{t+\Delta t}-[M][\ddot{x}]_{t+\Delta t}-[C][\dot{x}]_{t+\Delta t}-[\bar{P}]_{t+\Delta t}=0 \tag{4}$$

$$[\bar{P}]_{t+\Delta t}=[\bar{P}]_t+[K_T]_t([x]_{t+\Delta t}-[x]_t) \tag{5}$$

where Δt is the time step, $[F(t)]_{t+\Delta t}$ is the column vector of wind load related to the wind pressure distribution of structure at the time $t+\Delta t$, and $[K_T]_t$ denotes the tangential stiffness matrix computed by nodal displacements at time t.

The nonlinear term in the Eq. (3) is linearized by the Eq. (5). In this study, the discrete motion differential equation is solved by Newmark method, and Newton-Raphson iterative method is adopted to deal with the error problem caused by linearization (Zhang *et al*. 2014).

2.3 Calculation of equivalent damping coefficient

In this work, only the structural damping is considered in the calculation of the structural dynamic response, and Rayleigh damping model is a widely used orthogonal damping model for describing structural damping. The expression is as follows

$$[C]=\alpha[M]+\beta[K] \tag{6}$$

where α is the proportionality constant linking the damping to the mass, and it can be ignored in the actual engineering. β is the proportionality constant linking the damping to the stiffness, and it can be computed by the known values ξ_i and ω_i, namely

$$\beta=2\xi_i/\omega_i \tag{7}$$

where the structural damping ξ_i is generally taken as 1% (Jonkman *et al*. 2009). ω_i is the ith order response frequency of the structure, which is usually taken as the first order natural frequency. In this work, the first order natural frequencies of the whole machine model and the single blade model are obtained by computation, and they are respectively 0.14602 Hz and 0.3745 Hz, so the response frequencies are determined.

Assume that the displacement response of the blade at maximum displacement point $(\hat{x}, \hat{y}, \hat{z})$ is $\bar{w}(\hat{x}, \hat{y}, \hat{z}, t)$, and then one can obtain the dynamic equation of the equivalent dynamic system, that is (Zheng *et al.* 2001)

$$\ddot{\bar{w}}(\hat{x}, \hat{y}, \hat{z}, t)+2\omega_i\hat{\xi}\dot{\bar{w}}(\hat{x}, \hat{y}, \hat{z}, t)+\omega_i^2\bar{w}(\hat{x}, \hat{y}, \hat{z}, t)=0 \tag{8}$$

where $\hat{\xi}$ is the damping coefficient with respect to the displacement response.

The maximum displacements of two adjacent periods $\hat{T}$ are denoted as $\bar{w}_k(\hat{x}, \hat{y}, \hat{z}, t)$ and $\bar{w}_{k+1}(\hat{x}, \hat{y}, \hat{z}, t)$. Accordingly, the exponential attenuation coefficient $\hat{\delta}_k$ is expressed as

$$\hat{\delta}_k=\ln\left|\frac{\bar{w}_k(\hat{x}, \hat{y}, \hat{z}, t)}{\bar{w}_{k+1}(\hat{x}, \hat{y}, \hat{z}, t)}\right|=\hat{\xi}_k\omega_i\hat{T}\approx 2\pi\hat{\xi}_k \tag{9}$$

where k is the number of period. Hence, the damping coefficient can be obtained by

$$\hat{\xi}_k\approx\frac{\hat{\delta}_k}{2\pi} \qquad (k=1,2,\ldots) \tag{10}$$

Table 1 Parameters of 5MW wind turbine

Parameter	Value	Parameter	Value
Blade Number	3	Nacelle Mass	2.4×10^5 kg
Rotor Diameter	126 m	Blade Material	GFRP
Hub Diameter	3 m	Tower Material	Q345
Hub Height	90 m	Diameter of Tower Bottom	6 m
Rotor Mass	1.1×10^5 kg	Diameter of Tower Top	3.87 m

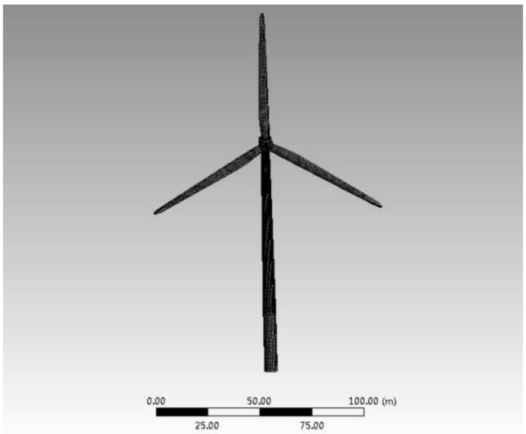

Fig. 1 Three-dimensional entity model and grid partition

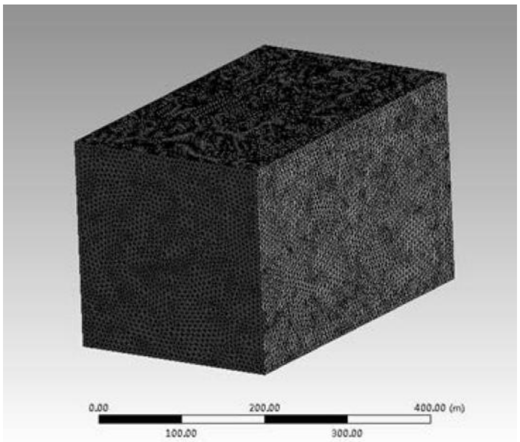

Fig. 2 External flow field

3. Finite element model

3.1 Entity modeling and grid partition

The main structure and physical parameters of 5MW offshore wind turbine provided by literature (Jonkman *et al.* 2009) are listed in Table 1. The entity model of wind turbine was constructed by the 3D modeling software UG, and the finite element software ANSYS was used to generate the grids of this model, as shown in Fig. 1.

In order to consider the rotating effect, a rotating domain model of the flow field was built to avoid the numerical calculation failure caused by problems involving the dynamic mesh damage in the process of structure rotation. The whole machine model was imported into the Geometry module of ANSYS Workbench, and an external flow field and an internal flow field formed by revolving around the rotating shaft were established. Note that the diameter and length of the internal flow field are 140 m and 25 m, respectively.

With the aim of really reflecting the interaction between the wind turbine structure and the surrounding flow field, the physical model of external flow field at the same proportion with the actual flow field was established in this

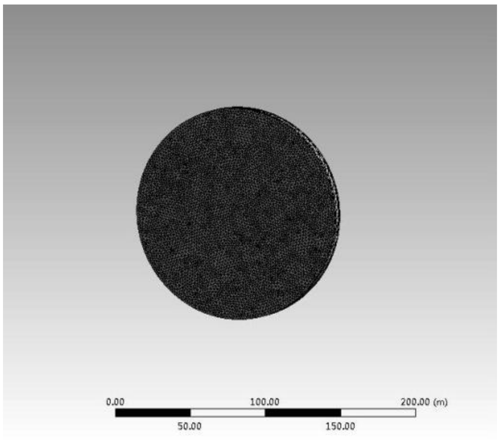

Fig. 3 Internal flow field

Table 2 Mesh independent verification

Mesh Unit Number	226735	334570	460550	517768
Maximum Displacement	3.08 m	2.75 m	2.59 m	2.52 m
Relative error	——	12.00%	6.17%	2.78%

work. In this model, the length of inflow region is equal to that of the rotor diameter, and the length of wake region is three times that of the rotor diameter. The cross section of the flow field perpendicular to the wind direction is a square, and the length of its side is twice that of rotor diameter. The established external flow field and the rotating domain are shown in Figs. 2 and 3 respectively.

3.2 Boundary conditions of fluid domain

The boundary conditions of fluid domain include inlet, outlet and wall boundary conditions, ect. In general, wind speed at infinity is set as inlet boundary condition at the inlet. Owing to the relatively large size of the fluid domain model in wind direction, the outlet boundary condition of pressure is chosen, and the atmospheric pressure is set at the outlet. For the wall boundary condition, the wind is treated as the viscous fluid, and the fluid speed on the wall is set to 0 m/s. Therefore, no slip and no penetration conditions are used near the surface, and upper, lower, front and rear boundaries are set as the wall. In addition, the standard k-epsilon equation is selected as turbulence model.

3.3 Mesh independent verification

The verification of mesh independence is one of the key steps affecting the accuracy of finite element computation. The maximum displacement of the blade top of the wind turbine is chosen to verify the correctness of mesh division. The verification results are listed in Table 2. It can be seen that a better calculation precision is obtained by using 517768 meshes. This mesh division is used in this study to save computational resources.

4. Reliability validation

In order to verify the accuracy of the theoretical model in this study, a single blade scaled model simplified from the whole machine model was designed and constructed for the wind tunnel test. The proportional scaling model of NREL 5 MW blade with the length of 700 mm was selected as the wind tunnel test model, and the blade was made by taking shape once in a high-precision numerical control machining center. The blade material is 6061T6 duralumin, and its parameters are listed in Table 3. In addition, the blade model is shown in Fig. 4.

The dynamic signal testing and analyzing system TST5912 and piezoresistance acceleration sensor TST220-050 were selected as test equipments. The distribution of sensors on the scaled blade model is shown in Fig. 5.

The connection between the sensor and the test system is displayed in Fig. 6. The basic principles of the test are as follows: First, use the bridge circuit to supply power for the acceleration sensor. Then turn on the dynamic signal test switch. Finally, record flapping acceleration response values of blade at different positions along the wingspan under the set wind speed.

In addition, the single blade scaled model was introduced into the FSI numerical program of this study, and the distribution of the flapping acceleration on blade surface along the wingspan was obtained at the wind speed of 30.2 m/s. The comparative curves of calculated values and experimental values are plotted in Fig. 7. It is observed that the variation trends of the two acceleration curves are consistent, and the comparative result shows a reasonable agreement as a whole, while near the blade root, the relative error is bigger than that at the blade tip, as a result of the fact that acceleration sensor has a low accuracy when the

Fig. 4 The scaled model of NREL 5MW blade

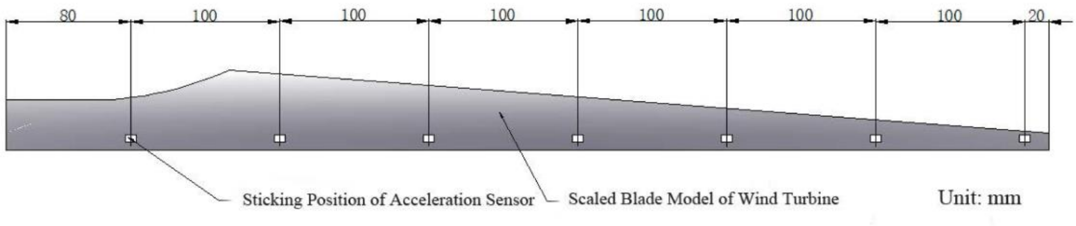

Fig. 5 Distribution of acceleration sensors

Fig. 6 Connection between sensor and test system

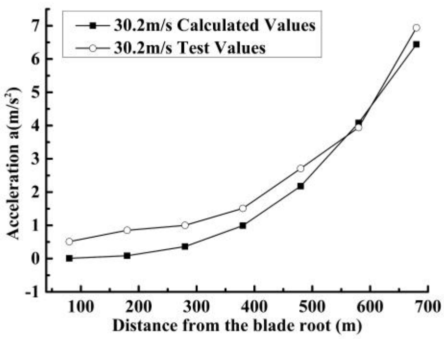

Fig. 7 Acceleration distribution of flapping direction along the wingspan

Table 3 The material parameters of 6061T6 duralumin

Elastic Modulus (GPa)	Poisson Ratio	Density (g/cm^3)
68.90	0.33	2.70

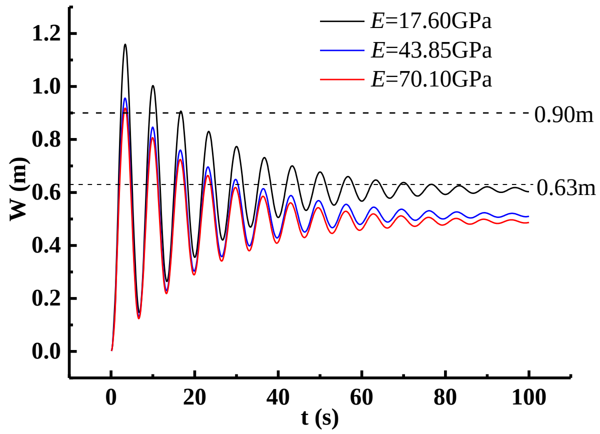

Fig. 8 Attenuation curves of blade maximum displacement for whole machine model

acceleration is less than $1.0\ m/s^2$. The comparative result near the blade top shows a good agreement, implying that the reading of the sensor is more accurate with the acceleration increasing, which verifies the reliability of the numerical procedure in this work.

5. Numerical results and discussions

On the basis of whole machine model, for the blade with different elastic modulus under the rated rotating speed of 12.1 rpm and the average wind speed of 11.4 m/s, the values of maximum displacement are calculated and the corresponding attenuation curves are drawn in Fig. 8. It is easily found from Fig. 8 that the blade maximum displacement is obviously nonlinear attenuation, and the peak value of maximum displacement basically meets the law of exponential attenuation, meaning that the maximum displacement response of the blade gradually tends to be stable with the increase of periods. What's more, it can be concluded by comparing the time of three attenuation curves decreasing from 0.90 m to 0.63 m that the attenuation of blade displacement becomes faster with the increasing elastic modulus. This can be interpreted as the reason that the increase of the elastic modulus causes the increase of stiffness, and then results in the rise of damping.

The equivalent damping coefficient of the wind turbine blade in Fig. 8 is determined by using Eqs. (9) and (10). Fig. 9 depicts the changing curves of the equivalent damping coefficient with the number of periods under different elastic modulus and their contrast curves. It can be obtained that the changing curves of equivalent damping coefficient all present a nonlinearly decreasing trend with increasing periodic number and the decreasing rate reduces continuously. At the initial stage of periods, the difference in the equivalent damping coefficients of blades with different elastic modulus is great and has a certain randomness, but finally approaches zero with the increase of period. According to the above conclusion, if the damping coefficient is set as a constant in actual engineering, it will lead to a certain range of errors in the structural dynamic calculation. Only by considering the situation that damping coefficient changes with the vibration period, can the dynamic attenuation characteristics of structure be more really reflected.

For the single blade model under the same working condition with whole machine model, the displacement attenuation curves of blade with different elastic modulus are plotted in Fig. 10 (a) to 10(c), respectively. It is found by comparing Fig. 8 with Fig. 10 that the blade vibration period of single blade model is significantly less than that of whole machine model. With the increase of elastic modulus, the difference of the blade maximum displacement between two models reduces gradually, and due to both damping variation and modal frequency shift, the variation of attenuation trend in the single blade model is more evident than that in whole machine model.

Under different elastic modulus, the varying curves of equivalent damping coefficient in the single blade with the number of periods are given in Fig. 11. One can obtain that the equivalent damping coefficient of the single blade attenuates faster with the increase of elastic modulus, and the difference under different elastic modulus decreases firstly and then increases with the increasing periods.

With the view of observing the structure coupling effect intuitively, the contrast results between Figs. 9 and 11 are plotted in Fig. 12. It can be seen that the attenuation rate of equivalent damping coefficient of single blade model is obviously less than that of whole machine model. When the

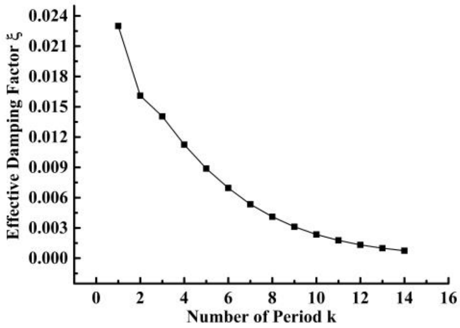

(a) $E = 17.60\,\text{GPa}$

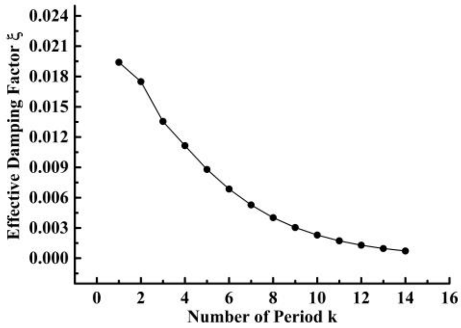

(b) $E = 43.85\,\text{GPa}$

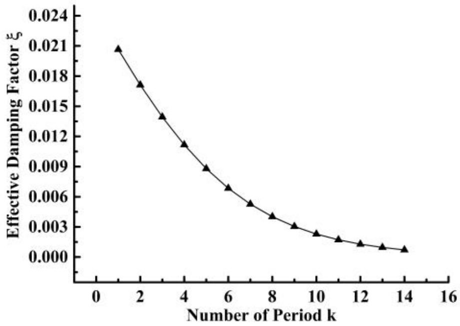

(c) $E = 70.10\,\text{GPa}$

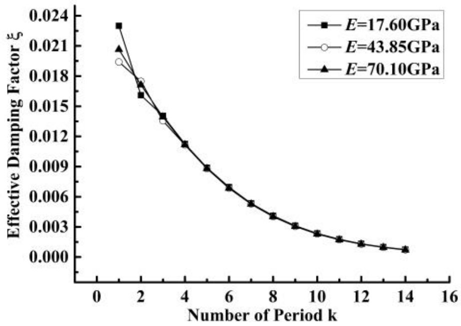

(d) Contrast curve

Fig. 9 The varying curves of equivalent damping coefficient in whole machine model

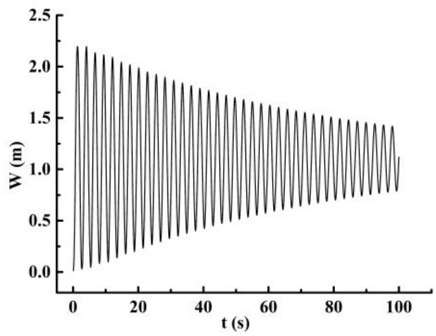

(a) $E = 17.60\,\text{GPa}$

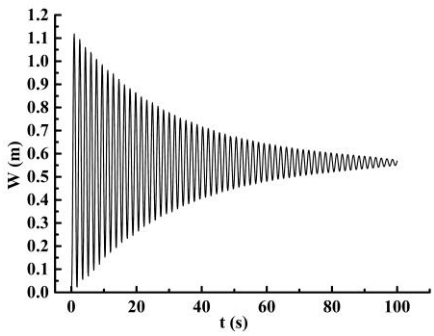

(b) $E = 43.85\,\text{GPa}$

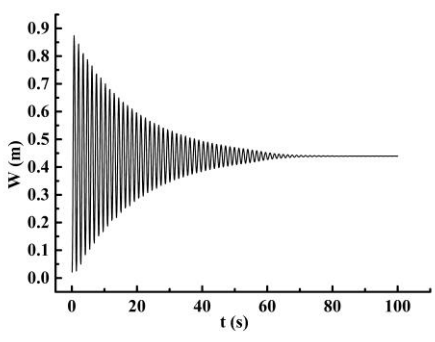

(c) $E = 70.10\,\text{GPa}$

Fig. 10 The attenuation curve of maximum displacement of single blade

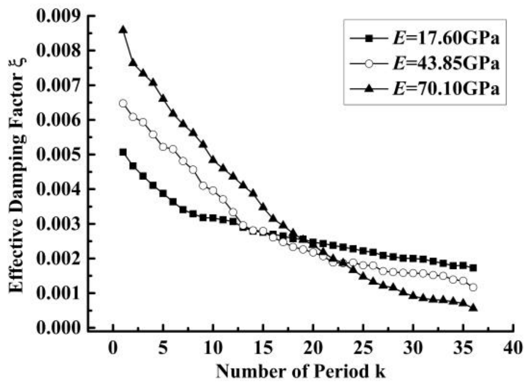

Fig. 11 The varying curves of equivalent damping coefficient of single blade model

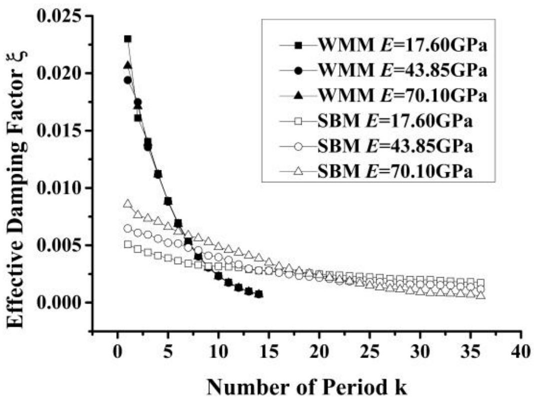

Fig. 12 The comparison of equivalent damping coefficients for two models

period ranges from 1 to 14, there exists a great difference in the equivalent damping coefficients of single blade model with different elastic modulus, while the difference is slight for the whole model, and under the same period and elasticity modulus, the equivalent damping coefficient of single blade model is smaller than that of whole machine model, but the former will exceed the latter with the increase of periods.

6. Conclusions

For 5 MW offshore wind turbines, the wind tunnel test based on the blade scaled model was conducted to verify the reliability of the calculation program in this study, and the blade equivalent damping coefficients of single blade model and whole machine model under different elastic modulus were computed by the attenuation curves of blade maximum displacement. The attenuation law of the blade dynamic response and the influence rule of the structure coupling effect on the equivalent damping coefficient are both revealed, and the followings can be summarized.

(1) The response curves of blade maximum displacement show an obviously nonlinear attenuation trend, and the peak value basically conforms to the rule of exponential attenuation. It can be proved that the response curve is in accordance with the underdamping vibration. The greater the elastic modulus of the blade material, the faster the displacement decreases, for the reason that the increase of elastic modulus results in the increase of stiffness, which thereby leads to the increase of damping, but for the single blade model, the fast displacement attenuation also depends on modal frequency shift.

(2) Under different elastic modulus, the equivalent damping coefficient of blade decreases nonlinearly with increasing periodic number, and the declining rate decreases gradually.

(3) The blade vibration period of single blade model is obviously smaller than that of whole machine model. With the increase of elastic modulus, the difference of blade maximum displacement between two models decreases constantly, and the attenuation trend of maximum displacement varies remarkably for the single blade, whereas it is basically unchanged under the structure coupling effect.

(4) For the models of single blade and whole machine, the varying curves of equivalent damping coefficient of single blade with the increasing periods are relatively smooth. Within the period range of the whole machine model, the difference of the equivalent damping coefficient

of single blade with different elastic modulus is more distinct than that under the structure coupling effect, and when elastic modulus is the same, the equivalent damping coefficient of the former is lower than that of the latter, but the opposite result appears with the increase of periods. It can be seen that the equivalent damping coefficient of the whole machine decreases sharply with the period due to the structure coupling effect, which is obviously different from the general damping system.

Acknowledgments

This study was financially sponsored by various research funds including the Program of Foundation of Science and Technology Commission of Shanghai Municipality (18DZ1202105, 18DZ1202302); National Natural Science Foundation of China (11572187).

References

Basu, B., Zhang, Z.L. and Nielsen, S.R.K. (2016), "Damping of edgewise vibration in wind turbine blades by means of circular liquid dampers", *Wind Energy*, **19**(2), 213-226. https://doi.org/10.1002/we.1827.

Chen, B., Zhang, Z., Hua, X., Nielsen, S.R.K. and Basu, B. (2017), "Enhancement of flutter stability in wind turbines with a new type of passive damper of torsional rotation of blades", *J. Wind Eng. Ind. Aerod*., **173**, 171-179. https://doi.org/10.1016/j.jweia.2017.12.011.

Eichler, A., Moser, J., Chaste, J., Zdrojek, M., Wilson-Rae, I. and Bachtold, A. (2011), "Nonlinear damping in mechanical resonators made from carbon nanotubes and graphene", *Nat. Nanotechnol*., **6**(6), 339-342. https://doi.org/10.1038/nnano.2011.71.

Jonkman, J., Butterfield, S., Musial, W. and Scott, G. (2009), "Definition of a 5-Mw Reference Wind Turbine for Offshore System Development", Report No. NREL/TP-500-38060; National Renewable Energy Laboratory, Golden, CO.

Liu, X., Li, G.Q., Chen, Y., Ye, Z.Q. and Tian, P. (2013), "Dynamic response analysis of the tubular tower of horizontal axis wind turbines", *Acta Energiae Solaris Sinica*, **31**(4), 412-41.

Lu, Z., Chen, X. and Zhou, Y. (2018), "An equivalent method for optimization of particle tuned mass damper based on experimental parametric study", *J. Sound Vib.*, **419**, 571-584. https://doi.org/10.1016/j.jsv.2017.05.048.

Magalhaes, F., Cunha, A., Caetano, E. and Brincker, R. (2010), "Damping estimation using free decays and ambient vibration tests", *Mech. Syst. Signal Pr*., **24**(5), 1274-1290. https://doi.org/10.1016/j.ymssp.2009.02.011.

Meng, J. and Sun, D.G. (2017), "Research on vibration suppression of wind turbine blade based on bamboo wall three-layer damping structure", *J. Vibroeng.*, **19**(1), 87-99. doi: 10.21595/jve.2016.17378.

Pascu, V., Kanev, S. and Van Wingerden, J. (2017), "Adaptive tower damping control for offshore wind turbines", *Wind Energy*, **20**(5), 765-781. https://doi.org/10.1002/we.2058.

Quan, Y., Cao, H.L. and Gu, M. (2016), "Effects of turbulence intensity and exterior geometry on across-wind aerodynamic damping of rectangular super-tall buildings", *Wind Struct.*, **22**(2), 185-209. https://doi.org/10.12989/was.2016.22.2.185.

Ren, Y.S. and Liu, T.R. (2013), "Stall nonlinear flutter of wind turbine blade modeled as thin-walled composite beam integrated with structural damping", *Appl. Mech. Mater.*, **291-294**, 496-500. https://doi.org/10.4028/www.scientific.net/AMM.291-294.496.

Tran, T.T. and Kim, D.H. (2015), "The coupled dynamic response computation for a semi-submersible platform of floating offshore wind turbine", *J. Wind Eng. Ind. Aerod.*, **147**, 104-119. https://doi.org/10.1016/j.jweia.2015.09.016.

Zendehbad, M., Chokani, N. and Abhari, R.S. (2017), "Measurements of tower deflections on full-scale wind turbines using an opto-mechanical platform", *J. Wind Eng. Ind. Aerod.*, **168**, 72-80. https://doi.org/10.1016/j.jweia.2017.05.011.

Zhang, D.Y., He, Y.F., Chen, L.L., Ma, Y.H. and Hong, J. (2016), "Theoretic investigation on vibration characteristics of structure with air film damper", *J. Aerosp. Power*, **31**(2), 282-288.

Zhang, F.H. and He, R. (2015), "Influence of structural damping on vibration property of tower of wind turbine", *Acta Energiae Solaris Sinica*, **36**(10), 2467-2473.

Zhang, J.P., Guo, L., Wu, H., Zhou, A.X., Hu, D.M. and Ren, J.X. (2014), "The influence of wind shear on vibration of geometrically nonlinear wind turbine blade under fluid–structure interaction", *Ocean Eng.*, **84**(4), 14-19. https://doi.org/10.1016/j.oceaneng.2014.03.017.

Zhang, Z.X. and Dong, Z.N. (1998), *Viscous Fluid Mechanics*, Tsinghua University Press, Beijing, CN.

Zheng, X.J., Zhou, Y.H. and Kenz, M. (2001), "An analysis of variable magnetic damping of a cantilever beam-plate with end coils in transverse magnetic fields", *Fusion Eng. Des*., **55**(4), 457-465. https://doi.org/10.1016/S0920-3796(01)00219-8.

FR

Nomenclature

ρ	Density of fluid
u_{gi}	Movement speed of grid in fluid domain
S_j	Generalized source term
$[x]_t$	Displacement at the time t
$[M]$	Mass matrix
$[C]$	Damping matrix
$[F(t)]$	Column vector of load on structure
$[K_T]_t$	Tangential stiffness matrix computed by nodal displacements at time t
α	Proportionality constant linking the damping to the mass
k	Number of period